

## 2 **On adaptive definition of the plane wave basis for wave** 3 **boundary elements in acoustic scattering: the 2D case**

4 **J. Trevelyan<sup>1</sup> and G. Coates<sup>1</sup>**

5 **Abstract:** The terminology “wave boundary elements” relates to boundary ele-  
6 ments enriched in the Partition of Unity sense by a multiple plane wave basis for the  
7 analysis of the propagation of short wavelength waves. This paper presents a vari-  
8 ant of this approach in which the plane wave basis is selected adaptively according  
9 to an error indicator. The error indicator is residual based, and exhibits useful lo-  
10 cal and global properties. Model improvement in each adaptive iteration is carried  
11 out by the addition of new plane waves with no  $h$ -refinement. The convergence  
12 properties of the scheme are demonstrated.

13 **Keywords:** wave scattering, plane wave basis, boundary integral equation, bound-  
14 ary elements, adaptivity.

### 15 **1 Introduction**

16 This paper deals with the efficient solution of frequency domain boundary value  
17 problems in wave propagation. Finite element and boundary element schemes have,  
18 of course, become well established as tools to carry out such simulations. However,  
19 users of conventional schemes, i.e. those schemes using a polynomial shape func-  
20 tion basis, are well known to be constrained by a heuristic rule that prescribes a  
21 maximum nodal spacing of approximately  $\lambda/10$ , where  $\lambda$  is the wavelength un-  
22 der consideration. Similar restrictions are found in meshless methods, e.g. Soares  
23 (2009). This places a de facto upper bound on the frequency that may be considered  
24 for any given problem given a finite computational resource. For many problems of  
25 practical scientific and engineering interest, e.g. radar scattering by an aircraft, this  
26 limitation presents an obstacle to the effective usage of element-based methods.

27 Attempts to increase the upper bound on frequency have been the subject of ac-  
28 tive research over the last decade. Fast multipole methods (FMM) (Chew, Jin,  
29 Michielssen, and Song (1997); Darve (2000), for example) present a promising  
30 avenue of research. For a problem containing  $N$  nodes, the  $N^2$  nodal interactions

---

<sup>1</sup> School of Engineering & Computing Sciences, Durham University, UK.

31 through the Green's function are expanded in a multipole expansion so that the total  
32 number of computations is greatly reduced, and giving rise to acceleration in  
33 the matrix vector products that are central to the iterative solution of large systems.  
34 Adaptive Cross Approximation (ACA) (Bebendorf (2000)) is an alternative technique  
35 for accelerating boundary element matrices for general applications; this has  
36 been applied to wave problems by Brancati, Aliabadi, and Benedetti (2009). The  
37 matrix is partitioned hierarchically in such a way that each partition may be accurately  
38 expressed as a low rank approximation implemented as a convergent series  
39 of vector operations.

40 Without prejudice against FMM and ACA, both of which are likely to be orthogonal  
41 to the methods presented herein, the current paper focuses on a class of methods  
42 in which the wave potential is sought in some wave basis. Abboud, Nédélec,  
43 and Zhou (1995) showed that, for convex scatterers impinged by an incident wave  
44 of sufficiently high frequency, the scattered potential may be efficiently approximated  
45 as the product of a slowly varying function and the incident wave itself.  
46 The slowly varying function may then be approximated using a piecewise polynomial  
47 finite element or boundary element space. This has been shown to provide  
48 "wavenumber independent" complexity, e.g. Bruno, Geuzaine, Munro, and Reitich  
49 (2004) present results for scatterers of dimension  $10^6\lambda$ . Langdon and Chandler-  
50 Wilde (2006) show that the approach is suitable for polygonal scatterers. Anand,  
51 Boubendir, Ecevit, and Reitich (2006) extended the approach to scattering by two  
52 or more objects. Dominguez, Graham, and Smyshlyaev (2007) showed that, for  
53 asymptotically high wave numbers, the number of degrees of freedom needs to  
54 grow only with  $\mathcal{O}(k^{1/9})$  to maintain a fixed error bound (the reader is reminded  
55 that wave number  $k = 2\pi/\lambda$ ). It should be recalled that these methods are limited  
56 to convex scatterers and may not perform well if  $\lambda$  is not very small in comparison  
57 with the scatterer, i.e. for low or medium frequency problems.

58 The extension of these ideas to consider a basis comprising multiple plane waves  
59 was proposed, without confirming examples, by de la Bourdonnaye (1994) for integral  
60 equation methods in wave simulation. The Partition of Unity Method (PUM)  
61 of Melenk and Babuška (1996) generalised the use of approximation spaces comprising  
62 sets of functions known to populate the solution space for any differential  
63 equation under consideration. Sets of plane waves were proposed for wave problems.  
64 When applied to finite element and boundary element approximations for waves,  
65 the PUM results in a reformulation of the problem so that we no longer  
66 seek the solution in terms of the nodal values of potential, but instead solve for  
67 the amplitudes of a set of approximating plane waves at each node that may be  
68 linearly combined to recover the potential field. Papers describing the Partition of  
69 Unity Finite Element Method (PU-FEM) for wave problems have appeared in the

70 literature, including Laghrouche, Bettess, and Astley (2002); Laghrouche, Bettess,  
71 Perrey-Debain, and Trevelyan (2003); Ortiz and Sanchez (2000), and the approach  
72 is also seen in the discontinuous enrichment method (see, for example, Farhat,  
73 Harari, and Franca (2001); Massimi, Tezaur, and Farhat (2008)), the generalized  
74 finite element method of Strouboulis, Babuška, and Hidajat (2006), the ultraweak  
75 variational formulation of Cessenat and Després (1998) and the Variational Theory  
76 of Complex Rays (VTCR) of Riou, Ladevèze, and Sourcis (2008). Following the  
77 initial proposition by de la Bourdonnaye (1994) of a multiple plane wave basis in  
78 a boundary integral equation, the approach was further developed in a series of pa-  
79 pers by Perrey-Debain, Trevelyan, and Bettess (2002, 2003a,b) and Perrey-Debain,  
80 Laghrouche, Bettess, and Trevelyan (2004), considering Helmholtz problems and  
81 elastic waves. These authors showed that the plane wave expansion reduced the  
82 required number of degrees of freedom to approximately 2.5 per wavelength, a  
83 marked reduction over the 10 per wavelength required with the polynomial basis  
84 while retaining ‘engineering accuracy’, as defined by 1%  $L^2(\Gamma)$  norm of the rel-  
85 ative error in comparison with an analytical solution. The inclusion of the PUM  
86 in a boundary element context may be termed PU-BEM, and the elements that are  
87 enriched in this way may be termed wave boundary elements.

88 Although recent advances have been made in the numerical integration of oscil-  
89 latory functions (Huybrechs and Vandewalle (2006); Trevelyan (2007); Honnor,  
90 Trevelyan, and Huybrechs (2009); Trevelyan and Honnor (2009); Kim, Dominguez,  
91 Graham, and Smyshlyaev (2009)), the run time in the PU-BEM is dominated by the  
92 evaluation of boundary integrals. It becomes important, therefore, to optimise care-  
93 fully the number of plane waves used in the basis at each node to minimise the total  
94 number of boundary integrals required to be considered. For general problems, in  
95 which an analytical solution is not available and the optimal local enrichment varies  
96 over the scatterer boundary, an adaptive scheme appears attractive for definition of  
97 the basis. Some initial experiments were reported at conferences by Trevelyan,  
98 Bettess, and Perrey-Debain (2004) for the PU-BEM and by Ladevèze, Sourcis,  
99 Riou, and Faverjon (2008) for the Variational Theory of Complex Rays (VTCR).  
100 Chandrasekhar and Rao (2008) have presented adaptive edge basis functions for a  
101 Method of Moments solution for acoustic scattering. This paper presents a fuller  
102 exposition of adaptivity in PU-BEM with appropriate error indicators.

103 Section 2 of this paper presents the PU-BEM for Helmholtz problems, and Sec-  
104 tion 3 presents the adaptive scheme that is the main novel component of the work.  
105 Section 4 contains some more detailed notes on implementation of the algorithms.  
106 Section 5 describes some results for two test cases, and some concluding remarks  
107 are made in Section 6.

## 108 2 Partition of Unity Boundary Element Method for wave propagation

109 We consider a domain  $\Omega \in \mathbb{R}^2$ , unbounded in the exterior and bounded internally  
 110 by a scatterer of boundary  $\partial\Omega = \Gamma$ . Assuming  $e^{-i\omega t}$  time dependence, the wave  
 111 equation reduces to the familiar Helmholtz equation form

$$(\nabla^2 + k^2)\phi(x) = 0, \quad x \in \Omega \quad (1)$$

112 where  $\nabla^2$  is the Laplacian operator,  $k$  is the wavenumber, given by  $2\pi/\lambda$ , and we  
 113 seek the complex potential field  $\phi(x)$ . This paper is aimed specifically at problems  
 114 characterised by medium to large  $k$ , such that the frequency is sufficiently high  
 115 that conventional FEM and BEM formulations become impractical, but not so high  
 116 that asymptotic methods apply. Let the scatterer be impinged by an incident wave  
 117  $\phi^I(x) = A^I e^{ik\psi^I \cdot x}$ , i.e. a plane wave of amplitude  $A^I \in \mathbb{C}$  travelling in the direction  
 118 described by unit vector  $\psi^I$ . Transformation of the governing differential equation  
 119 into an equivalent boundary integral equation (BIE) form is standard (e.g. Brebbia  
 120 and Ciskowski (1991)), arriving at

$$c(x_0)\phi(x_0) + \int_{\Gamma} \frac{\partial G(x, x_0)}{\partial n} \phi(x) d\Gamma(x) = \int_{\Gamma} G(x, x_0) \frac{\partial \phi(x)}{\partial n} d\Gamma(x) + \phi^I(x_0), \quad x_0 \in \Gamma \quad (2)$$

where  $c$  is a scalar dependent on the boundary geometry at point  $x_0$ ,  $n$  is the unit  
 outward-pointing normal at boundary point  $x$ , and  $G$  is the Green's function, which  
 for the Helmholtz equation is given by

$$G(x, x_0) = \frac{i}{4} H_0(kr). \quad (3)$$

121 Here  $r := |x - x_0|$  is the usual radial coordinate in boundary element methods, and  
 122  $H_0(\cdot)$  is a Hankel function of the first kind and of order 0. Considering a general  
 123 form of boundary condition to be applied, given by

$$\frac{\partial \phi(x)}{\partial n} = \alpha(x)\phi(x) + \beta(x), \quad x \in \Gamma \quad (4)$$

the BIE may be reformulated as

$$c(x_0)\phi(x_0) + \int_{\Gamma} \left( \frac{\partial G(x, x_0)}{\partial n} - G(x, x_0)\alpha(x) \right) \phi(x) d\Gamma(x) = \int_{\Gamma} G(x, x_0)\beta(x) d\Gamma(x) + \phi^I(x_0)$$

(5)

Here, for compact presentation we take the case of a perfectly reflecting (“sound-hard”) scatterer, so  $\alpha(x) = \beta(x) = 0, x \in \Gamma$ , leading to a BIE in only the double layer potential,

$$c(x_0)\phi(x_0) + \int_{\Gamma} \frac{\partial G(x, x_0)}{\partial n} \phi(x) d\Gamma(x) = \phi^I(x_0). \quad (6)$$

However, the approach extends in an identical fashion to sound-soft or impedance boundary conditions. In the direct collocation BEM, the boundary  $\Gamma$  is discretised and each element of boundary  $\Gamma_e$  considered in an intrinsic coordinate system through the usual parameterisation of a finite/boundary element, i.e.

$$\Gamma_e = \{\gamma_e(\xi) : \xi \in [-1, 1]\} \quad (7)$$

where  $\gamma_e : \mathbb{R} \rightarrow \mathbb{R}^2$ . For any element, the mapping between  $x \in \Gamma$  and  $\xi$  is unique and bidirectional, and it shall be henceforth assumed that any function  $f(x)$  is equivalent to  $f(\xi)$  as suggested by this mapping. Expressing the potential in a piecewise polynomial basis over element  $e$ ,

$$\phi(x) = \sum_{j=1}^J N_j(x) \phi_j^e \quad (8)$$

where  $J$  is the number of nodes per element,  $N_j$  is the Lagrangian shape function for node  $j$  and  $\phi_j^e$  is the unknown nodal potential at node  $j$  on element  $e$ , we write

$$c(x_0)\phi(x_0) + \sum_{e=1}^E \sum_{j=1}^J \int_{-1}^{+1} \frac{\partial G(x, x_0)}{\partial n} N_j(\xi) J^n(\xi) d\xi \phi_j^e = \phi^I(x_0) \quad (9)$$

where  $E$  is the total number of elements, and  $J^n$  is the Jacobian of the mapping (7). Collocating this discretised statement of the BIE at a sufficient number of points  $x_0 \in \Gamma$  yields a system of linear equations that may be solved for the nodal potentials in the conventional fashion. Some method needs to be employed to overcome the problem posed by the non-uniqueness of the solution to (6) at the eigenfrequencies of the associated interior Dirichlet problem (Schenck (1968); Burton and Miller (1971)); the current authors use the method of Schenck (1968) for reasons of computational efficiency but modified in a similar fashion to Mohsen and Hesham (2006) to retain a square system. To move from the classical direct collocation BEM to the PU-BEM, we introduce the plane wave expansion of the potential on an element  $e$ ,

$$\phi(x) = \sum_{j=1}^J N_j(x) \sum_{m=1}^M A_{jm}^e e^{ik\psi_{jm}^e \cdot x}, \quad |\psi_{jm}^e| = 1 \quad (10)$$

where  $A_{jm}^e \in \mathbb{C}$  and  $\psi_{jm} \in \mathbb{R}^2$  are, respectively, the amplitudes and directions of the plane waves in the basis. For nodes that are shared between adjacent elements, the same plane wave basis is considered for each element, and the amplitudes of the individual waves are taken to be identical, providing for  $C^0$  continuity in potential across element interfaces.  $M$  may be chosen such that, for any given mesh, requirements on the number of degrees of freedom per wavelength,  $\tau$ , are observed both globally and locally. We recall that  $\tau \geq 10$  is generally observed for FEM and BEM approximations; Perrey-Debain, Trevelyan, and Bettess (2003a) have shown that a considerably coarser discretisation of  $\tau \simeq 2.5$  is sufficient for PU-BEM. In general,  $\tau$  may be allowed to reduce further towards 2.0 as the frequency increases. Substitution of (10), instead of (8), into (6) results in the BIE being reformulated such that the unknowns become the amplitudes  $A_{jm}^e$ .

$$c(x_0)\phi(x_0) + \sum_{e=1}^E \sum_{j=1}^J \sum_{m=1}^M \int_{-1}^{+1} \frac{\partial G(x, x_0)}{\partial n} N_j(\xi) e^{ik\psi_{jm}^e \cdot x} J^n(\xi) d\xi A_{jm}^e = \phi^I(x_0) \quad (11)$$

There become  $M$  degrees of freedom associated with each node, and so collocation only at the nodes will provide an insufficient number of equations; an auxiliary set of equations is provided by collocating at a sufficient number of non-nodal points distributed over the boundary. To accomplish this, the potential at the collocation point,  $\phi(x_0)$ , in (11) needs to be written in the expansion (10),

$$\phi(x_0) = \sum_{j=1}^J N_j(x_0) \sum_{m=1}^M A_{jm}^{\bar{e}} e^{ik\psi_{jm}^{\bar{e}} \cdot x_0} \quad (12)$$

where  $\bar{e}$  is the element on which  $x_0$  lies. This yields a square system of linear equations

$$[W + K] \{a\} = \{b\} \quad (13)$$

where the sparse square matrix  $W$  results from interpolation of the plane waves through (12) and square matrix  $K$  is fully populated with the boundary integrals contained in (11). Right hand side vector  $b$  contains the incident wave potentials at the collocation points, and the unknown vector  $a$  contains the amplitudes  $A_{jm}^e$ . The amplitudes may be determined through solution of the system (13), being careful to use a solver appropriate to the conditioning of  $[W + K]$ , and the potential field may quickly be recovered through (10). If required, solutions in the domain  $\Omega$  (e.g. for the far-field pattern) may be found by making further use of (11) in the usual way. In most PU-BEM works in the literature, and cited in this article, the wave directions  $\psi_{jm}^e$  have been simply defined to be equally spaced around the unit circle,

i.e.

$$\psi_{jm}^e = (\cos\theta_{jm}^e, \sin\theta_{jm}^e), \quad \theta_{jm}^e = \frac{2\pi(m-1)}{M} + \delta\theta \quad (14)$$

124 In order to represent the physical optics solution for large  $k$ , we take the offset  
 125  $\delta\theta$  to be the direction of the incident wave. We note that, while the number of  
 126 waves,  $M$ , is generally much more important than the direction vectors  $\psi_{jm}^e$ , the  
 127 results do exhibit some sensitivity to the basis directions chosen. Selection of a  
 128 wave basis that is in some sense optimal for the problem in question is an open  
 129 research question (see Bériot, Perrey-Debain, Ben Tahar, and Vayssade (2010)).  
 130 In the following section we show how this set of wave directions is augmented  
 131 iteratively to enhance the solution.

### 132 3 Adaptive scheme

The core elements of most adaptive schemes found in the FE and BE literature are an error indicator and some strategy, generally  $h$  or  $p$ , for model improvement. The current work is no exception. This section presents such a scheme, of the  $p$ -adaptive character, for 2D PU-BEM approximations. In this scheme, the number of plane waves in the basis at node  $j$  of element  $e$ , now denoted  $M_{ej}$ , varies with  $j$ . Thus the BIE (11) may be presented in the slightly modified form,

$$c(x_0)\phi(x_0) + \sum_{e=1}^E \sum_{j=1}^J \sum_{m=1}^{M_{ej}} \int_{-1}^{+1} \frac{\partial G(x, x_0)}{\partial n} N_j(\xi) e^{ik\psi_{jm}^e \cdot x} J^n(\xi) d\xi A_{jm}^e = \phi^I(x_0) \quad (15)$$

133 In successive iterations of the adaptive scheme, the approximation space is progres-  
 134 sively enriched by the addition of plane waves by incrementing the value  $M_{ej}$  at any  
 135 node(s) selected by a local error indicator.

A residual based error indicator  $R$  may be defined as,

$$R(x_1) := \frac{1}{|A^I|} \left| c(x_1)\phi(x_1) + \int_{\Gamma} \frac{\partial G(x, x_1)}{\partial n} \phi(x) d\Gamma(x) - \phi^I(x_1) \right|, \quad x_1 \in \Gamma \quad (16)$$

where the integral term may be evaluated in the same discrete form as in (15)

$$\int_{\Gamma} \frac{\partial G(x, x_1)}{\partial n} \phi(x) d\Gamma(x) \equiv \sum_{e=1}^E \sum_{j=1}^J \sum_{m=1}^{M_{ej}} \int_{-1}^{+1} \frac{\partial G(x, x_1)}{\partial n} N_j(\xi) e^{ik\psi_{jm}^e \cdot x} J^n(\xi) d\xi A_{jm}^e \quad (17)$$

We note that when Dirichlet and/or impedance boundary conditions are used the single layer potential term must also be included in the computation of the error

indicator. Having solved the system for the amplitudes  $A_{jm}^e$ , the potentials  $\phi(x)$  and  $\phi(x_1)$  are available by recombination from (10), and the entire right hand side of (16) may be readily evaluated to give the error indicator at an arbitrary boundary point  $x_1$ .  $R$  may be expected to be close to zero-valued when evaluated at  $x_1 = x_0$ , one of the original set of collocation points used in the solution of the problem. Typical behaviour is illustrated in Figure 1, in which the variation in  $R$  is plotted over one line element containing 13 uniformly distributed collocation points;  $R$  can be seen to be considerably lower at the original set of collocation points than at other locations on the element. The error indicator reaches a maximum approximately midway between each pair of collocation points  $x_0$ . It is further noticed consistently that the peaks in  $R$  increase towards the extremities of the element, a feature we attribute to the fact that the shape functions exhibit only  $C^0$  continuity at the element boundaries. Therefore we consider the behaviour of  $R$  over an element  $e$  to be reasonably described by its value at just two points,  $x_L^e$  and  $x_R^e$ . These points are defined by their locations in parametric space, i.e.

$$\xi(x_L^e) = \frac{1}{2}(\xi(x_{0L}) + \xi(x_L)) \quad (18)$$

$$\xi(x_R^e) = \frac{1}{2}(\xi(x_{0R}) + \xi(x_R)) \quad (19)$$

- 136 where  $x_L$  and  $x_R$  are the two end node locations, and  $x_{0L}, x_{0R}$  are the non-nodal collocation points on the element that are closest to  $x_L$  and  $x_R$  respectively.

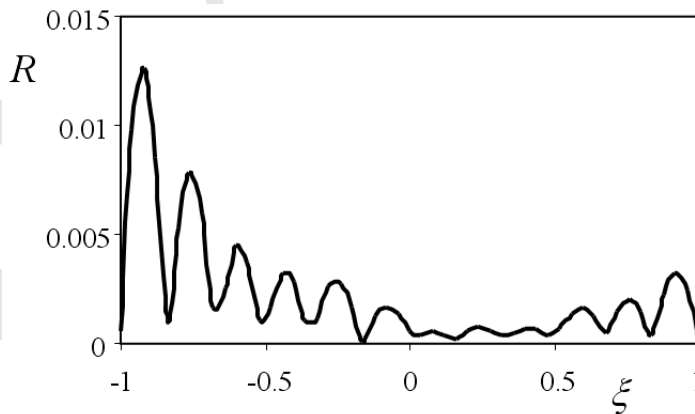
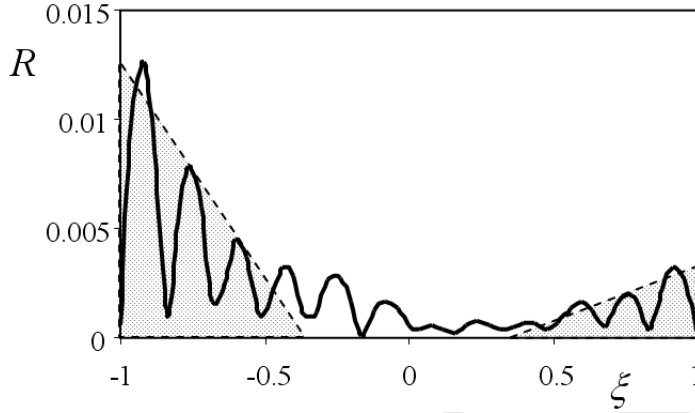


Figure 1: Behaviour of error indicator over an element containing 13 collocation points


 Figure 2: Showing the algorithm for approximating  $\|R\|_1$ 

A suitable global error indicator might be based on a norm of  $R$ . Since  $R(x_1) \geq 0, \forall x_1 \in \Gamma$ , a 1-norm is sufficient, so that we define a global error norm

$$\|R\|_1 := \frac{1}{P} \oint R(x) d\Gamma(x) \quad (20)$$

where  $P$  is the perimeter of the boundary  $\Gamma$ . However, since it involves the evaluation of many highly oscillatory boundary integrals, this norm is costly to compute numerically. Fortunately, for the purpose of using it as a stopping criterion, the norm (20) is sufficiently well approximated by

$$\|R\|_1 \simeq \frac{1}{6P} \sum_{e=1}^E L^e [R(x_L^e) + R(x_R^e)] \quad (21)$$

where  $L^e$  is the length of element  $e$ . This corresponds to the combined area of the triangles of base equal to one third of the element length and height equal to  $R(x_L^e)$  and  $R(x_R^e)$ , as illustrated in Figure 2. Numerical tests suggest that, using the definition (21), a stopping criterion  $\|R\|_1 < 0.004$  is generally suitable to obtain engineering accuracy of 0.01 in  $\varepsilon$ , the  $L^2(\Gamma)$  relative error norm of the approximation for  $\phi$  for a perfectly reflecting cylinder, for which the exact solution,  $\phi^{ex}$ , is available in Morse and Feshbach (1981). Reducing the threshold value for the stopping criterion provides for improved accuracy of the converged solution. For completeness we define  $\varepsilon$  as

$$\varepsilon = \frac{\|\phi - \phi^{ex}\|_{L^2(\Gamma)}}{\|\phi^{ex}\|_{L^2(\Gamma)}} \quad (22)$$

138 In evaluating  $\|R\|_1$  using (21) it is important to store the local values of the error  
 139 indicator  $R(x_L^e), R(x_R^e), e = 1, \dots, E$  found at any of these sampling points, since they  
 140 will be used as the local error indicator.

Although it includes a non-local integral operator, the error indicator (16) may also be viewed as having local properties since it is effectively the use of the BIE to compute the potential  $\phi(x_1)$ , and evaluation of the discrepancy between this computation and the recovery of  $\phi(x_1)$  from the PU-BEM solution through (10). We can illustrate the effectiveness of local variation in  $R$  as a local error indicator using the perfectly reflecting cylinder. For a case in which 24 elements are used to model the cylinder, we computed for each element the values

$$\varepsilon^e = \frac{\|\phi - \phi^{ex}\|_{L^2(\Gamma_e)}}{\|\phi^{ex}\|_{L^2(\Gamma_e)}} \quad (23)$$

$$\|R\|_1^e = \frac{L^e}{6P} [R(x_L^e) + R(x_R^e)] \quad (24)$$

141 These values, normalised by the maxima  $\max(\varepsilon^e, e = 1, \dots, 24)$  and  $\max(\|R\|_1^e, e =$   
 142  $1, \dots, 24)$  are plotted in Figure 3. There is a clear correlation, which we interpret as a justification to use  $R$  as a local error indicator.

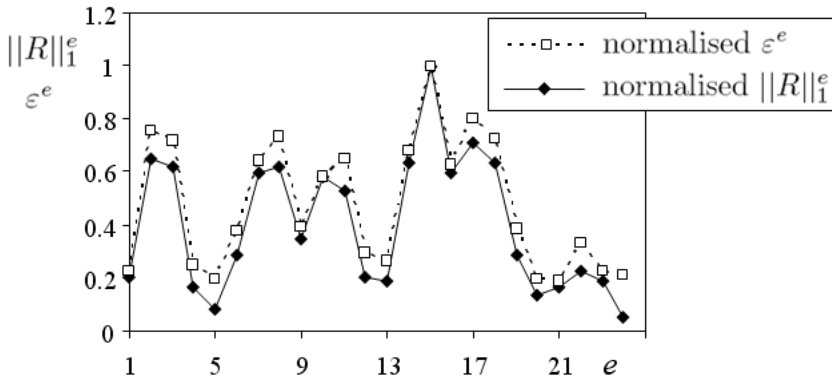


Figure 3: Variation of  $\varepsilon^e$  and  $\|R\|_1^e$  over a 24 element model

143

144 In each adaptive iteration, new waves are added to the approximation space at nodes  
 145 suggested by the local variation in the error indicator. New rows and columns are  
 146 appended to the system matrix and a new solution is obtained. In the current work,  
 147 since the evaluation of the boundary integrals incurs a large majority of the compu-  
 148 tational cost of the PU-BEM for typical problems, the complete set of equations is  
 149 solved at each adaptive iteration. Further work is justified in incremental solution

150 schemes that might be iterative or involve an updated decomposition of the grow-  
 151 ing system matrix. Such schemes are likely to require preconditioning. The major  
 152 benefit of the scheme is to end up with an approximation space that is optimised for  
 153 the problem at hand such that confidence is gained in the solution accuracy while  
 154 the number of oscillatory integral evaluations is effectively minimised.

#### 155 4 Implementation

156 Different strategies have been tested for the  $p$ -adaptive enrichment in response to  
 157 the local behaviour of  $R$ . It has been noted by Trevelyan, Bettess, and Perrey-  
 158 Debain (2004) that the residual error indicator lacks the characteristic smoothness  
 159 of Figure 1 when the plane wave basis is non-uniform. We suppose this to be an  
 160 artefact of some interference between the waves in the basis at different nodes.  
 161 The somewhat enhanced quality of the solution for a uniform basis is exploited in  
 162 the final algorithm, in which the following steps are carried out in each adaptive  
 163 iteration:

- 164 1. determine  $R(x_L^e), R(x_R^e), e = 1, \dots, E$  from (16) and, in the same process, as-  
 165 semble the global error norm  $\|R\|_1$  from (21).
- 166 2. if  $\|R\|_1 < 0.004$  the stopping criterion has been satisfied. Recover the poten-  
 167 tial solution from (10) and stop.
3. determine the total number of waves,  $n_u$ , that would be required to be added  
 in order to reach a uniform basis at all nodes. If the model is already at a  
 uniform basis,  $n_u$  takes the value of the total number of nodes, otherwise

$$n_u = \sum_{e=1}^E \sum_{j=1}^{J-1} M_{max} - M_{ej} \quad (25)$$

168 where  $M_{max} = \max(M_{ej}, e = 1, \dots, E, j = 1, \dots, J)$ .

- 169 4. make a list of all nodes adjacent to sampling points  $x_1 \in \{x_L^e, x_R^e, e = 1, \dots, E\}$   
 170 at which  $R(x_1) > R_{max}$ . Here,  $R_{max}$  is a threshold to be determined by numer-  
 171 ical tests. Let there be  $n_a$  such nodes in the list.
- 172 5. if  $n_a > 0.75n_u$  replace the list of nodes generated in step 4 by a list of  
 173 length  $n_u$ , generated in step 3, that would bring about a uniform basis  $M_{ej} =$   
 174  $M_{max}, e = 1, \dots, E, j = 1, \dots, J$ .
- 175 6. work down the list of nodes. At each, add a new wave in between two existing  
 176 plane waves such that the basis becomes  $\{e^{ik\psi_{jm}^e x}, m = 1, \dots, M_{ej} + 1\}$ , and  
 177 increment by 1 the value of  $M_{ej}$ .

- 178 7. define new collocation points in the same number as the added degrees of  
179 freedom.
- 180 8. evaluate the boundary integrals required to populate the new rows and columns  
181 in  $K$ .
- 182 9. update required entries in the sparse matrix  $W$  to include the contributions of  
183 the newly added waves.
- 184 10. solve the enlarged PU-BEM system (13) for all plane wave amplitudes.
- 185 11. return to step 1.

The initial plane wave basis at all nodes  $j$  on all elements  $e$  comprises  $M_{ej}^1$  wave directions uniformly spaced around the unit circle, i.e.

$$\psi_{jm}^e = (\cos\theta_{jm}^e, \sin\theta_{jm}^e), \quad \theta_{jm}^e = \frac{2\pi(m-1)}{M_{ej}^1} + \delta\theta, \quad m = 1, \dots, M_{ej}^1 \quad (26)$$

186 The value of  $M_{ej}^1$  is determined to give an appropriate meshing efficiency  $\tau \simeq 2.1$ ,  
187 where  $\tau$  is the number of degrees of freedom used to model a portion of boundary  $\Gamma$   
188 spanning one wavelength. We recall that  $\tau = 10$  is the usual heuristic rule for FEM  
189 and BEM approximations to wave problems using a piecewise polynomial basis.

190 At the start of the analysis, we initialise counting parameters  $p_{ej} = 1$ ,  $q_{ej} = 1$  for all  
191 nodes. The following algorithm is used in step 6 of subsequent adaptive iterations to  
192 define the direction of a single plane wave direction in between existing directions  
193 at a node.

1. introduce a new plane wave in a direction

$$\theta_{jm} = \frac{p_{ej}\pi}{q_{ej}M_{ej}^1} + \delta\theta \quad (27)$$

194 where  $m$  is taken as  $M_{ej}^1 + 1$ . The associated unit vector  $\psi_{jm}^e$  is defined as in  
195 (26), and  $M_{ej}^1$  is incremented by 1.

- 196 2. modify values of  $p_{ej}$  and  $q_{ej}$  according to:

- 197 (a) if  $p_{ej} + 2 < 2q_{ej}M_{ej}^1$ , then let  $p_{ej} = p_{ej} + 2$  and  $q_{ej} = q_{ej}$
- 198 (b) if  $p_{ej} + 2 \geq 2q_{ej}M_{ej}^1$ , then let  $p_{ej} = 1$  and  $q_{ej} = 2q_{ej}$

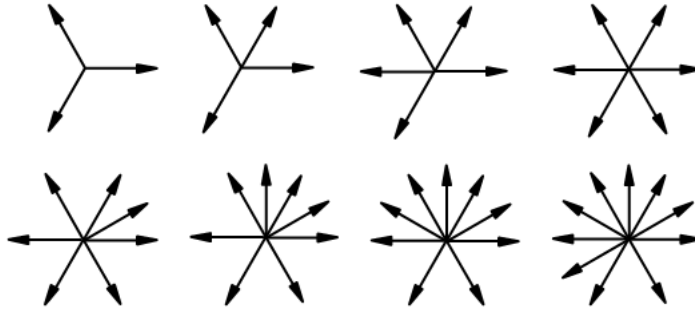


Figure 4: Progressive addition of waves (case  $M_{e_j}^1 = 3$  shown)

199 This algorithm sequentially adds waves to bisect adjacent pairs of waves and will  
 200 continue to find the next bisector at each new addition. This is illustrated in Figure  
 201 4 for the first eight iterations for the case  $M_{e_j}^1 = 3$ . Numerical tests have shown that  
 202 a moderate asymmetry of the plane wave basis is not detrimental to the solution  
 203 obtained.

204 At each iteration, in step 7 a set of additional collocation points is defined so that  
 205 the total number of collocation points is equal to the number of unknowns. We  
 206 locate the new points on the elements on which new plane waves are added, but  
 207 confine the new points to the interval  $\xi \in (\xi(x_{0L}), \xi(x_{0R}))$  in the present study in  
 208 order to maintain a consistent definition of the global error norm (21).

#### 209 4.1 Mesh considerations

It is clear from the presentation of the PU-BEM in Section 2, that the degrees of freedom in the analysis are represented by the amplitudes of a set of plane wave directions forming a basis for the approximation space at each node. Simple consideration of the perimeter,  $P$ , and of the required number of degrees of freedom per wavelength,  $\tau$ , will suggest that a total number of degrees of freedom,  $N_d$ , where

$$N_d = \frac{P\tau}{\lambda}, \quad (28)$$

210 should be provided. Let us assume, for simplicity, that every node is provided  
 211 with a uniform basis comprising  $M$  wave directions, and that there is a total of  $N$   
 212 nodes.  $N_d$  is then given by  $MN$ . Thus we have flexibility to accumulate the re-  
 213 quired number of degrees of freedom by various combinations of  $M$  and  $N$ . Early  
 214 developments in the PU-BEM for Helmholtz problems (Perrey-Debain, Trevelyan,  
 215 and Bettess (2003a)) showed that the accuracy of the method is influenced by this

216 choice, and concluded that convergence is optimised if  $N$  is minimised and  $M$  max-  
 217 imised. Best results were shown for  $N = 1$ , i.e. using a single element to model the  
 218 entire closed boundary.

219 With the introduction of adaptivity, we have a conflicting demand, since the algo-  
 220 rithm progresses by improving the model in a *localised* way. For this reason, we  
 221 proceed into Section 5 to present examples having a larger  $N$  and smaller  $M$  than  
 222 would be suggested by the 2003 study.

## 223 5 Results

224 The adaptive PU-BEM algorithm is illustrated in this section using two example  
 225 problems: scattering of a plane wave by a circular cylinder and by a system of  
 226 three cylinders of different diameters. The cylinders are perfectly reflecting as is  
 227 assumed for simplicity in the theoretical development earlier in this paper; for more  
 228 general cases the algorithm would simply be extended by including the single layer  
 229 potential in the residual error indicator (16).

### 230 5.1 Scattering by a circular cylinder

231 Consider a cylindrical scatterer of radius  $a = 10$  impinged by an incident wave of  
 232 unit amplitude and wavelength  $\lambda = 0.5$  (consistent units are assumed) propagating  
 233 in direction (1,0). This example provides  $ka = 125$ . The cylinder is modelled by  
 234 24, 3-noded boundary elements, and the initial model is provided with  $M_{ej}^1 = 6$   
 235 for all nodes, giving 288 degrees of freedom ( $\tau = 2.29$  degrees of freedom per  
 236 wavelength). This initial analysis has error norm  $\|R\|_1 = 0.00548$ . The adaptive  
 237 algorithm converges in a single further iteration to finish at  $\|R\|_1 = 0.00125$ , which  
 238 corresponds to a 0.33% error in the  $L^2(\Gamma)$  relative error norm on the potential solu-  
 239 tion in comparison with the analytical solution in Morse and Feshbach (1981). In  
 240 the converged solution the model has 313 degrees of freedom at  $\tau = 2.49$ . The total  
 241 run time is comparable to the non-adaptive solution using a uniform basis  $M = 7$ ;  
 242 in fact it shows a small reduction of 4% in run time.

243 The geometry-normalised wavenumber  $ka = 125$  in this example is sufficiently  
 244 high that the initial model, exhibiting  $\tau = 2.29$ , is itself able to produce a reason-  
 245 ably accurate solution. The adaptive procedure has fine-tuned the solution with a  
 246 more efficient use of resources than simply running again with a larger  $M$  applied  
 247 uniformly. If we retain the 24-element mesh but double the wavelength to give  
 248 a reduced  $ka = 62.8$ , the initial model exhibits  $M_{ej}^1 = 3$  for all nodes, giving 144  
 249 degrees of freedom ( $\tau = 2.29$  degrees of freedom per wavelength). Three adaptive  
 250 iterations are required in order to achieve convergence. In these three iterations  
 251 the global error norm is found to be 0.0124, 0.00401 (just missing the stopping

252 criterion) and 0.00210. Again, the run-time shows a small saving of 12.3% over  
 253 the most efficient non-adaptive solution that achieves the same accuracy using a  
 254 uniform basis. It is to be expected that the run times for adaptive and non-adaptive  
 255 solutions are comparable, since the gains that are made by reducing the number of  
 256 oscillatory integral evaluations are offset by the requirement to solve the system of  
 257 equations multiple times.

258 Figure 5 shows plots of  $R$  over the boundary  $\Gamma$  for the solutions of the three adaptive  
 259 iterations. In these graphs the horizontal axis is defined by angle  $\theta$  taken clockwise  
 260 around the scatterer, having  $\theta = 0$  at the first point of contact with the incident  
 261 wave. The asymmetry of the error indicator about  $\theta = \pi$  may be attributed to the  
 262 random definition of the Chief points inside the scatterer.

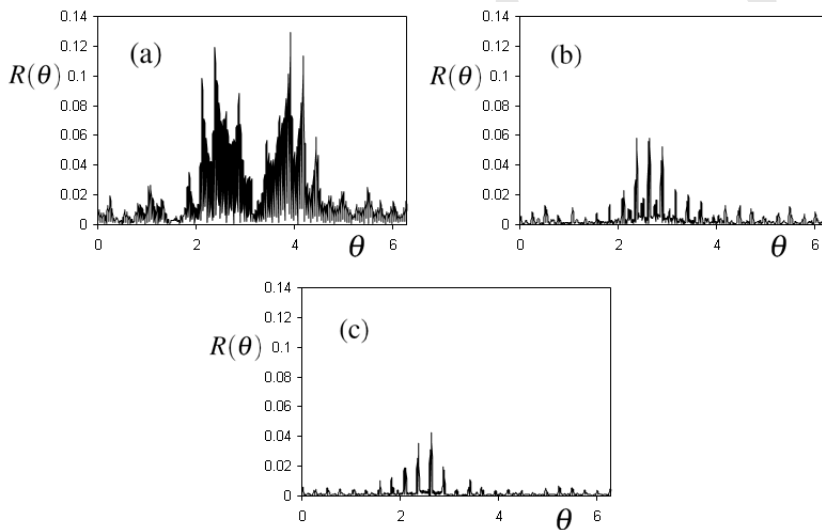


Figure 5: Evolution of error indicator for cylinder problem taking  $ka = 62.8$ . (a) first iteration, (b) second iteration, (c) third and final iteration

263 It should be noted that the calculation of  $R$  over the boundary, enabling the plotting  
 264 of Figure 5, is made for illustrative purposes only, and the reader is reminded that in  
 265 this scheme the error indicator is required only at two points per element, as shown  
 266 in equation (21).

267 For scattering by a single cylinder the behaviour of the PU-BEM is well understood  
 268 so that, using a non-adaptive solution using a uniform basis of  $M$  plane waves at  
 269 each node, it is possible to select a suitable value of  $M$  a priori that experience  
 270 suggests will give any desired accuracy. The principal advantage of the adaptive

271 scheme is found in more general problems, where the choice of an appropriate  
 272  $M$  is not so clear and cannot be deduced from experience as for a single cylinder  
 273 problem. We proceed now to present such a case.

## 274 5.2 Scattering by three cylinders

275 Consider a set of cylindrical scatterers in an infinite acoustic medium, being im-  
 276 pinged by an incident plane wave of unit amplitude and wavelength  $\lambda = 0.25$ ,  
 277 propagating in direction  $(1,0)$ . The geometry and meshing for the scatterers are  
 278 defined in Table 1. All elements have three nodes, and the entire boundary to the  
 279 problem,  $\Gamma$ , is defined as  $\Gamma = \Gamma_1 \cup \Gamma_2 \cup \Gamma_3$ .

Table 1: Geometric definition of the three cylinders

Scatterer	Centre	Radius	No. of elements	Boundary
1	(0, 0)	1	8	$\Gamma_1$
2	(2, 3)	2	16	$\Gamma_2$
3	(4, -2)	3	24	$\Gamma_3$

The convergence of the global error norm  $\|R\|_1$ , from  $\|R\|_1 = 0.1485$  for the initial analysis ( $M = 4, \tau = 2.54$ ) to achieve convergence in the 4th iteration at  $\|R\|_1 = 0.00264$ , is shown in Figure 6. Convergence is achieved using  $N_d = 631$  at  $\tau = 4.18$ . Contours of the converged solution  $Re(\phi)$  are shown in Figure 7, and show reflection from the illuminated surfaces, a clear shadow region to the right, diffraction around the sides of the scatterers and a complicated region of multiple reflections between the three cylinders. This complication is emphasised by plotting  $|\phi|$  on  $\Gamma_2$ , as shown in Figure 8. In Figure 9, we plot over  $\Gamma_2$  a measure,  $\epsilon_2$ , of the difference between the converged adaptive solution (plotted in Figure 8) and the solution  $\bar{\phi}$  obtained using a direct collocation BEM approximation using 1520 degrees of freedom at  $\tau = 10.1$ . This measure is defined by

$$\epsilon_2 = \frac{\| |\phi| - |\bar{\phi}| \|}{|\bar{\phi}|_{max}} \quad (29)$$

We can measure the improvement in accuracy as the adaptive scheme progresses using a relative error,  $\epsilon_3$ , defined as

$$\epsilon_3 = \frac{\| \phi - \bar{\phi} \|_{L^2(\Gamma)}}{\| \bar{\phi} \|_{L^2(\Gamma)}} \quad (30)$$

280 The evolution in  $\epsilon_3$  with iteration number is shown in Figure 10. The most efficient  
 281 non-adaptive solution to achieve this accuracy uses  $M = 7$  and exhibits  $\tau = 4.46$ . In

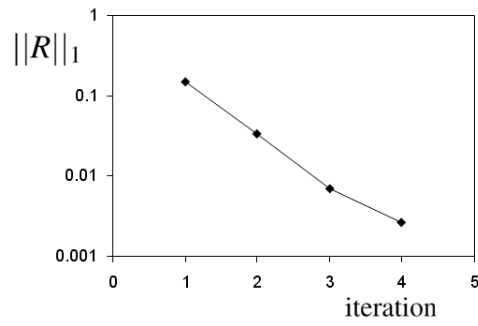


Figure 6: Evolution of global error norm for three cylinder problem

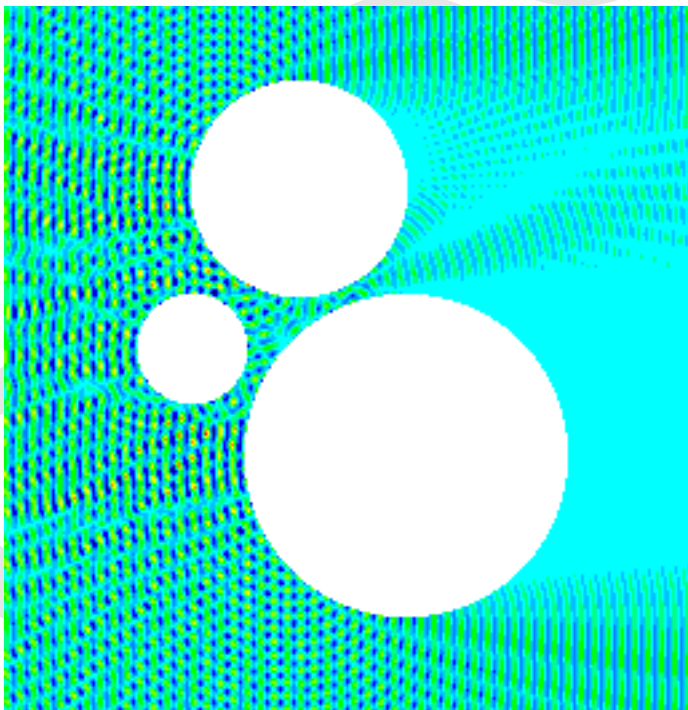


Figure 7: Real part of the potential (converged solution)

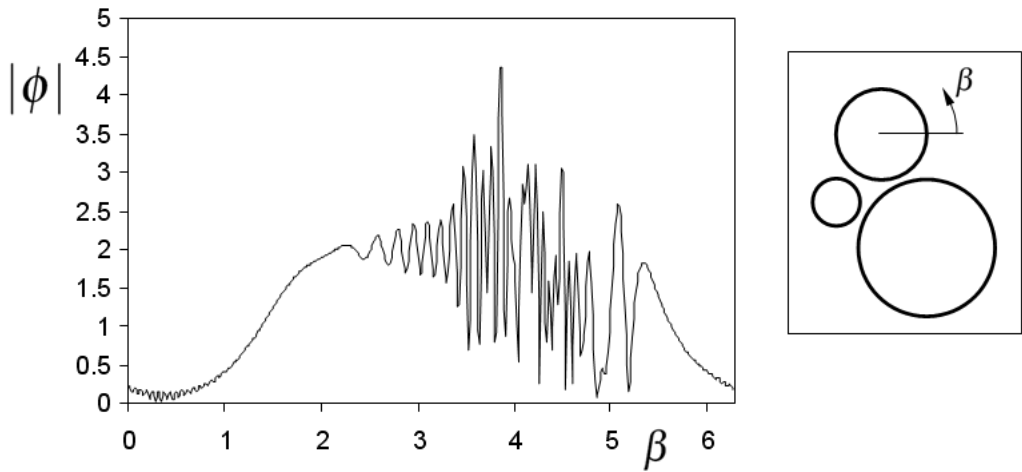


Figure 8: Magnitude of potential on boundary of scatterer 2

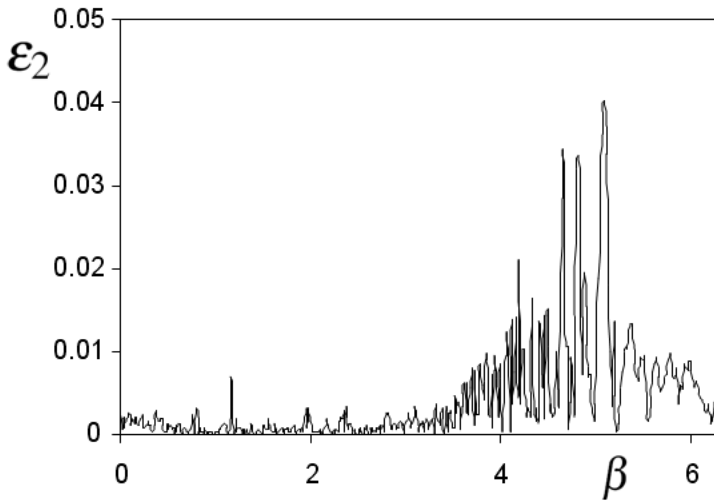


Figure 9: Difference measure  $\epsilon_2$  on boundary of scatterer 2

282 this case the run-time for the adaptive solution is somewhat greater (by 19%) than  
 283 this non-adaptive solution, but it must be remembered that the required value of  $M$   
 284 for non-adaptive solutions is not known in advance and that multiple runs may be  
 285 required to confirm convergence.

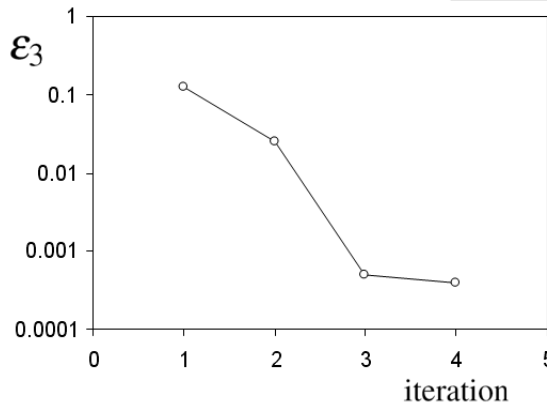


Figure 10: Evolution of  $\epsilon_3$  for three cylinder problem

## 286 6 Conclusions

287 An adaptive form of the Partition of Unity Boundary Element Method (PU-BEM)  
 288 has been presented for the solution of wave scattering problems. The approach  
 289 involves a residual based error indicator that has both global and local properties,  
 290 allowing it to be used as a stopping criterion and also as an indicator of areas of a  
 291 model in which further enrichment is required. The residual is normalised by the  
 292 amplitude of the incident wave in scattering problems, allowing a single threshold  
 293 to be used for general scattering problems. An efficient approximation to the global  
 294 error norm is presented, requiring evaluation at only two points on each element.

295 The adaptive scheme is of the p-adaptive character; the mesh remains unaltered but  
 296 the approximation space is enriched in each iteration, in regions suggested by the  
 297 local variation in the error indicator, by the addition of an extra plane wave to the  
 298 basis. An algorithm is presented for the iterative addition of new waves in between  
 299 existing wave directions.

300 Illustrative examples demonstrate the convergence of the algorithm to solutions  
 301 that exhibit at least engineering accuracy. More accuracy may be obtained simply  
 302 by modifying the threshold value for the global error norm that is used as a stop-  
 303 ping criterion. Run times for the adaptive solution are comparable to those of the

304 most efficient non-adaptive solution that achieves the same accuracy using a uni-  
 305 form basis. The adaptive scheme is beneficial in that it removes the requirement to  
 306 estimate in advance the required number of plane waves with which to enrich the  
 307 approximation space; such an estimate is not always straightforward.

308 Further work is required to extend the algorithm to scattering problems in 3D,  
 309 where greater benefits are expected.

## 310 References

311 **Abboud, T.; Nédélec, J.; Zhou, B.** (1995): Improvement of the integral equation  
 312 method for high frequency problems. In *3rd Intl. Conf. on Mathematical Aspects*  
 313 *of Wave Propagation Phenomena*, pp. 178–187. SIAM, Philadelphia.

314 **Anand, A.; Boubendir, Y.; Ecevit, F.; Reitich, F.** (2006): Analysis of mul-  
 315 tiple scattering iterations for high-frequency scattering problems. ii: The three-  
 316 dimensional scalar case. *Preprint 147/2006, Max Planck Institute*.

317 **Bebendorf, M.** (2000): Approximation of boundary element matrices. *Numer.*  
 318 *Math.*, vol. 86, pp. 565–589.

319 **Bériot, H.; Perrey-Debain, E.; Ben Tahar, M.; Vayssade, C.** (2010): Plane  
 320 wave basis in galerkin bem for bidimensional wave scattering. *Engineering Anal-*  
 321 *ysis with Boundary Elements*, vol. 34, pp. 130–143.

322 **Brancati, A.; Aliabadi, M.; Benedetti, I.** (2009): Hierarchical adaptive cross ap-  
 323 proximation gmres technique for solution of acoustic problems using the boundary  
 324 element method. *Computer Modeling in Engineering and Sciences*, vol. 43, pp.  
 325 149–172.

326 **Brebbia, C.; Ciskowski, R.** (1991): *Boundary Element Methods in Acoustics*.  
 327 CMP and Elsevier Applied Science, Southampton.

328 **Bruno, O.; Geuzaine, C.; Munro, J.; Reitich, F.** (2004): Prescribed error toler-  
 329 ances within fixed computational times for scattering problems of arbitrarily high  
 330 frequency: the convex case. *Phil. Trans. Royal Soc. London A*, vol. 362, no. 1816,  
 331 pp. 629–645.

332 **Burton, A.; Miller, G.** (1971): The application of integral equation methods to  
 333 the numerical solution of some exterior boundary-value problems. *Phil. Trans.*  
 334 *Royal Soc. London A*, vol. 323, pp. 201–210.

335 **Cessenat, O.; Després, B.** (1998): Application of the ultra-weak variational  
 336 formulation of elliptic pde's to the two-dimensional helmholtz problem. *SIAM J.*  
 337 *Numer. Anal.*, vol. 35, pp. 255–299.

- 338 **Chandrasekhar, B.; Rao, S.** (2008): A faster method of moments solution to double  
339 layer formulation of acoustic scattering. *Computer Modeling in Engineering and*  
340 *Sciences*, vol. 33, pp. 199–214.
- 341 **Chew, W.; Jin, J.; Michielssen, E.; Song, J.** (1997): Fast solution methods in  
342 electromagnetics. *IEEE Trans Antennas Propag*, vol. 45, pp. 533–543.
- 343 **Darve, E.** (2000): The fast multipole method: numerical implementation. *Journal*  
344 *of Computational Physics*, vol. 1608, pp. 195–240.
- 345 **de la Bourdonnaye, A.** (1994): A microlocal discretization method and its uti-  
346 lization for a scattering problem. *Comptes Rendus de l'Académie des Sciences.,*  
347 *Paris, Série I*, vol. 38, pp. 385–388.
- 348 **Dominguez, V.; Graham, I.; Smyshlyaev, V.** (2007): A hybrid numerical-  
349 asymptotic boundary integral method for high-frequency acoustic scattering. *Nu-*  
350 *mer. Math.*, vol. 106, pp. 471–510.
- 351 **Farhat, C.; Harari, I.; Franca, L.** (2001): The discontinuous enrichment  
352 method. *Computer Methods in Applied Mechanics and Engineering*, vol. 190,  
353 pp. 6455–6479.
- 354 **Honor, M.; Trevelyan, J.; Huybrechs, D.** (2009): Numerical evaluation of 2d  
355 partition of unity boundary integrals for helmholtz problems. *Journal of Compu-*  
356 *tational and Applied Mathematics*, vol. to appear.
- 357 **Huybrechs, D.; Vandewalle, S.** (2006): On the evaluation of highly oscillatory  
358 integrals by analytic continuation. *SIAM J. Numer. Anal.*, vol. 44, pp. 1026–1048.
- 359 **Kim, T.; Dominguez, V.; Graham, I.; Smyshlyaev, V.** (2009): Recent progress  
360 on hybrid numerical-asymptotic methods for high-frequency scattering problems.  
361 In *Proc. 7th UK Conf. on boundary integral methods*, pp. 15–23. Univ. of Notting-  
362 ham.
- 363 **Ladevèze, P.; Sourcis, B.; Riou, H.; Faverjon, B.** (2008): An adaptative compu-  
364 tational “wave” approach. In *Proc. WCCM8/ECCOMAS, Venice, Italy*.
- 365 **Laghrouche, O.; Bettess, P.; Astley, R.** (2002): Modelling of short wave diffrac-  
366 tion problems using approximating systems of plane waves. *International Journal*  
367 *for Numerical Methods in Engineering*, vol. 54, pp. 1501–1533.
- 368 **Laghrouche, O.; Bettess, P.; Perrey-Debain, E.; Trevelyan, J.** (2003): Plane  
369 wave basis finite elements for wave scattering in three dimensions. *Communica-*  
370 *tions in Numerical Methods in Engineering*, vol. 19, no. 9, pp. 715–723.

- 371 **Langdon, S.; Chandler-Wilde, S.** (2006): A wavenumber independent boundary  
372 element method for an acoustic scattering problem. *SIAM J. Numerical Analysis*,  
373 vol. 43, pp. 2450–2477.
- 374 **Massimi, P.; Tezaur, R.; Farhat, C.** (2008): A discontinuous enrichment method  
375 for three-dimensional multiscale harmonic wave propagation problems in multi-  
376 fluid and fluid-solid media. *International Journal for Numerical Methods in Engi-  
377 neering*, vol. 76, pp. 400–425.
- 378 **Melenk, J.; Babuška, I.** (1996): The partition of unity finite element method.  
379 basic theory and applications. *Computer Methods in Applied Mechanics and En-  
380 gineering*, vol. 139, pp. 289–314.
- 381 **Mohsen, A.; Hesham, M.** (2006): An efficient method for solving the nonunique-  
382 ness problem in acoustic scattering. *Communications in Numerical Methods in  
383 Engineering*, vol. 22, pp. 1067–1076.
- 384 **Morse, P.; Feshbach, H.** (1981): *Methods of Theoretical Physics*. Feshbach  
385 Publishing.
- 386 **Ortiz, P.; Sanchez, E.** (2000): An improved partition of unity finite element  
387 model for diffraction problems. *International Journal for Numerical Methods in  
388 Engineering*, vol. 50, pp. 2727–2740.
- 389 **Perrey-Debain, E.; Laghrouche, O.; Bettess, P.; Trevelyan, J.** (2004): Plane  
390 wave basis finite elements and boundary elements for three dimensional wave scat-  
391 tering. *Phil. Trans. Royal Society London A*, vol. 362, no. 1816, pp. 561–577.
- 392 **Perrey-Debain, E.; Trevelyan, J.; Bettess, P.** (2002): New special wave bound-  
393 ary elements for short wave problems. *Communications in Numerical Methods in  
394 Engineering*, vol. 18, no. 4, pp. 259–268.
- 395 **Perrey-Debain, E.; Trevelyan, J.; Bettess, P.** (2003): Plane wave approximation  
396 in the direct collocation boundary element method for radiation and wave scatter-  
397 ing: numerical aspects and applications. *Journal of Sound and Vibration*, vol. 261,  
398 no. 5, pp. 839–858.
- 399 **Perrey-Debain, E.; Trevelyan, J.; Bettess, P.** (2003): Wave boundary elements  
400 for acoustic computations. *Journal of Computational Acoustics*, vol. 11, no. 2, pp.  
401 305–321.
- 402 **Riou, H.; Ladevèze, P.; Sourcis, B.** (2008): The multiscale vcr approach applied  
403 to acoustics problems. *Journal of Computational Acoustics*, vol. 16(4), pp. 487–  
404 505.

- 405 **Schenck, H.** (1968): Improved integral formulation for acoustic radiation prob-  
406 lems. *Journal of the Acoustical Society of America*, vol. 44, pp. 41–58.
- 407 **Soares, D.** (2009): Numerical modelling of electromagnetic wave propagation by  
408 meshless local petrov-galerkin formulations. *Computer Modeling in Engineering*  
409 *and Sciences*, vol. 50, pp. 97–114.
- 410 **Strouboulis, T.; Babuška, I.; Hidajat, R.** (2006): The generalized finite element  
411 method for helmholtz equation: Theory, computation and open problems. *Com-*  
412 *puter Methods in Applied Mechanics and Engineering*, vol. 195, pp. 4711–4731.
- 413 **Trevelyan, J.** (2007): Numerical steepest descent evaluation of 2d partition  
414 of unity boundary integrals for helmholtz problems. *Oberwolfach Report*, vol.  
415 *5/2007*, pp. 74–76.
- 416 **Trevelyan, J.; Bettess, P.; Perrey-Debain, E.** (2004): Experiments in adaptive  
417 selection of plane wave basis directions for wave boundary elements. In *Develop-*  
418 *ments in Mechanics of Structures and Materials*.
- 419 **Trevelyan, J.; Honnor, M.** (2009): A numerical coordinate transformation for ef-  
420 ficient evaluation of oscillatory integrals over wave boundary elements. *J. Integral*  
421 *Equations and Appl.*, vol. 21, pp. 447–468.
- 422 **Acknowledgement:** This work has been funded by the Engineering and Physical  
423 Sciences Research Council (EPSRC), under grant GR/C511026/1, whose support  
424 is gratefully acknowledged. We also acknowledge the helpful work of Mr. Miguel  
425 Garcia.